High-beta bursts in SMA mediate anticipatory muscle inhibition in a bimanual motor task

V. Manyukhina, O. Abdoun, F. Di Rienzo, F. Barlaam, S. Daligault, C. Delpuech, M. Bonnefond, C. Schmitz

High-beta bursts in SMA mediate anticipatory muscle inhibition in a bimanual motor task

V. Manyukhina[1], O. Abdoun[1], F. Di Rienzo[1,2], F. Barlaam[1], S. Daligault[3], C. Delpuech[1,3], M. Bonnefond[1]*, C. Schmitz[1]*

*both authors equally contributed to the work

[1]Lyon Neuroscience Research Center (CRNL), Computation, Cognition and Neurophysiology Team (Cophy), INSERM
UMRS 1028, CNRS UMR 5292, Université de Lyon, Université Claude Bernard Lyon 1, Lyon, France
[2]Laboratoire Interuniversitaire de Biologie de la Motricité, Université de Lyon, Université Claude Bernard Lyon 1, Lyon, France
[3]Département Magnétoencéphalographie, CERMEP Imagerie du Vivant, Bron, France

Abstract

In motor networks, motor inhibition can be driven by sensorimotor mu rhythm (8-12Hz) or beta bursts (13-30Hz). In this study, we aimed to investigate whether mu or beta activity supports efficient anticipatory inhibition, as reflected by a decrease in electromyographic (EMG) activity. To test this, we recorded magnetoencephalography (MEG) in 16 adults performing a Bimanual Load Lifting Task (BLLT), where participants lifted a load with one hand supported by the other. In anticipation of unloading, elbow flexors in the supporting arm are inhibited to prevent elbow deflection. We observed that optimal postural stabilization occurs when flexor inhibition happens approximately 30 ms before unloading begins. Stronger EMG inhibition in this time interval correlated negatively with high-gamma power (90-130Hz), reflecting reduced neural excitability, and positively with high-beta power in the medial supplementary motor area (SMA). In contrast, no significant correlation was observed in the mu-range (8-12 Hz). Meanwhile, high-beta and high-gamma power were negatively correlated. Mediation analysis confirmed that gamma power significantly mediates the relationship between beta power and EMG inhibition. Beta burst probability and directed connectivity analysis using the Phase Slope Index indicated that high-beta bursts are transmitted from the middle prefrontal cortex (mPFC) and elbow-related primary motor cortex (M1) to the SMA. Our findings suggest that, in the voluntary unloading task, anticipatory muscle inhibition at the optimal time is driven by a reduction in excitability within the SMA, likely facilitated by high-beta bursts originating from the mPFC-M1-SMA network.

Significance

Anticipatory motor processes represent a form of higher-order motor control evolved in humans to enable precise hand manipulation. In this study, we used a bimanual coordination task where precise force control is achieved by sending an inhibitory motor command to the elbow flexors before an anticipated forearm disturbance, which requires accurate timing and pattern selection. We demonstrate that timely anticipatory inhibition is associated with the transmission of high-beta bursts (22-28Hz) to the supplementary motor area, suppression of which enables precise inhibitory control over the flexor muscle. These findings suggest the neural mechanisms underlying anticipatory postural control and provide the first direct evidence linking beta activity to muscle inhibition.

Introduction

Many voluntary movements cause postural perturbations that can be anticipated by adjusting postural muscles before movement (Massion, 1992). A common example is the “waiter task”: when a waiter holds a tray of glasses and is about to take one with his other hand, the brain must adapt to the upcoming force changes on the tray-bearing arm to avoid spillage. This behaviour is achieved through anticipatory postural adjustments (APA), which are integral to our daily lives and are required for most rapid arm and leg movements (Stone et al., 2014; Kane & Barden, 2012).

A commonly used naturalistic paradigm for studying APA in humans is the bimanual weight lifting task (BLLT), mimicking the waiter example (Hugon et al., 1982). In BLLT, a load is placed on the wrist of the left, postural arm, with the elbow fixed to allow only up-down rotation, while the participant lifts the load using the right, motor arm.The unloading causes a force imbalance, leading to destabilization of the postural arm, observed as upward forearm movement. When a subject moves voluntarily, APA precedes the lifting, stabilizing the forearm serving as a reference frame, which results in minimal deflection. In contrast, unexpected unloading causes a pronounced upward elbow rotation, followed by reflexive inhibition that stabilizes posture (Hugon et al, 1982).

APA results from precise brain-level coordination between the postural and motor arms, which requires engaging the same muscles to support and lift the load (Massion, 1992; Kaluzny et al., 1992). Another integral feature of APA is inhibition of elbow flexor activity, reflected as decreased electromyography (EMG) signal. This inhibition precedes unloading, anticipating forearm imbalance, and presumably reflects the suppression of established wrist stabilisation during load maintenance. Thus, anticipatory inhibition ensures a smooth transition to a new equilibrium, and its timely realisation is crucial for effective bimanual coordination (Hugon et al., 1982; Viallet et al., 1987). Impaired APA, measured with the BLLT, has been observed in Parkinson’s disease (Viallet et al., 1987), autism spectrum disorder (Schmitz et al., 2003), and other motor-related conditions (Jover et al., 2006; Jover et al., 2010).

The network and mechanisms underlying anticipatory inhibition, distinct from its behavioural outcome of elbow stabilisation, have not been thoroughly investigated. Studying them, particularly during BLLT, is advantageous for several reasons. First, it can help us better understand the neural mechanisms involved in transitioning between motor commands. Second, unlike many motor inhibition paradigms, BLLT offers direct insight into the mechanisms of neural inhibition, given an explicit EMG-based measure. Together, a better understanding of these mechanisms may provide valuable insights into the neural pathways underlying motor deficits in patients.

Additionally, due to the spatial separation between hemispheric effects related to arm movement and posture, BLLT provides a unique opportunity to study anticipatory postural control in bimanual coordination.

In motor networks, inhibition can be mediated by mu (8-12Hz) or beta (13-30Hz) activity. Stronger mu power facilitates active inhibition of information processing in motor networks (Bönstrup et al., 2015; Karabanov et al., 2021; Köster & Meyer, 2023). Beta oscillations, predominantly in the form of bursts (Lundqvist et al., 2024), have been linked to inhibition of motor actions (Picazio et al., 2014; Schaum et al., 2021; Enz et al., 2021) or their slowing (Khanna & Carmena, 2017), but are also strengthened during tonic muscle contraction (Kilavik et al., 2013).

In this study, we aimed to investigate the neural pathways responsible for anticipatory inhibition and the oscillatory mechanisms underlying this process. Based on prior research on BLLT and motor inhibition (Kazennikov et al., 2006; Ng et al., 2013; Borgomaneri et al., 2020), we hypothesized that anticipatory elbow flexor inhibition in BLLT is linked to a decrease in M1 excitability. This decrease, in turn, may be triggered by an inhibitory signal expressed at alpha or beta frequencies, originating from the prefrontal cortex or subcortical brain regions such as the basal ganglia or cerebellum.

Methods

Participants

Sixteen right-handed adults without neurological or psychiatric conditions (11 males, mean age 27 ± standard deviation (SD) 3.8 years) participated in this study. Handedness was determined using the Edinburgh Handedness Inventory (Oldfield, 1971). All participants gave written informed consent in accordance with the Declaration of Helsinki. The study was approved by the local ethics committee (South East IV Committee for the Protection of Persons). A study involving the same participants and describing the results of a different task has previously been published (Rienzo et al., 2019).

Experimental setting and task

The experimental setup for the voluntary unloading situation in the BLLT was described in more details elsewhere (Massion et al. 1999; Barlaam et al. 2011; Rienzo et al., 2019). In short, a wooden table was placed in front of a participant that allowed the right arm to be comfortably placed on it. The left arm was chosen as the postural

arm, and was positioned adjacent to the trunk with a support, with the elbow being fixed to allow only upward and downward rotations. The subject was instructed to maintain the left forearm in a horizontal semi-prone position, which served as a reference. A metal wristband fitted with a vacuuming switch system (30 kN/m^2) strain gauge was worn on the wrist which allowed a load of 850g to be placed on the top of it (in the voluntary unloading setup of BLLT), or to be suspended with a possibility to be released by means of 3.5 kN/m^2 air pulses (in the imposed unloading setup).

In the voluntary (natural) unloading, each trial started with a 2 second fixation on an LED located at the base of the load in order to avoid eye movements. Subjects had to lift the load placed on top of the wristband with their right hand at any time after the light faded out. After a few seconds of maintenance, subjects had to return the load in the initial position, which finalized the trial. As the unloading was performed by the participants themselves, this allowed anticipation and resulted in very small elbow destabilization following unloading. This condition is also expected to be characterized by anticipatory EMG inhibition in the elbow flexor muscles (Biceps Brachii and Brachioradialis), which typically occurs just before the onset of unloading (Viallet, 1987; Paulignan, 1989; Barlaam et al., 2011).

In the imposed (control) unloading condition, the load was released at an unpredictable time initiated by the experimenter in each trial, making anticipation impossible. The imposed unloading results in a visible upward rotation of the elbow and passive, reflex-like EMG inhibition in the elbow flexor muscles, which begins after the unloading (Viallet, 1987; Paulignan, 1989; Barlaam et al., 2011).

In total, there were 90 trials in both imposed and voluntary unloading conditions. To reduce fatigue, they were organised into sessions of 10 trials each, with intervals of around 1 minute between the sessions.

Behavioural data acquisition

Detection of load-lifting timing

The onset of load-lifting (unloading, zero reference time point) was automatically identified as the initial deflection in the force signal recorded by the force plate sensor attached to the metallic wristband, using a threshold function in CTF® DataEditor software. The automatically assigned label was then visually inspected and manually corrected if needed.

Elbow-joint rotation

Upward rotation of the elbow joint following load release or load lifting was measured across all trials and conditions using a potentiometer aligned with the elbow joint axis, sampled at 600 Hz. The deflection strength was recorded in arbitrary units provided by the equipment.

Electromyography

Electromyography (EMG) data were collected at a sampling frequency of 600 Hz using bipolar surface electrodes (2.5 mm^2 surface area) positioned over the left Brachioradialis, Biceps Brachii, and Triceps Brachii, as well as the right Biceps Brachii. For the purposes of this study, only EMG data from the left Biceps Brachii were analyzed.

Behavioural data preprocessing

Elbow rotation

To assess the postural stabilization as a measure of efficacy of anticipatory postural control, we estimated two measures: Peak Elbow Rotation and Elbow Rotation Decline, which reflect whether the posture was stable after and before the unloading, respectively (see Figure 2A, left panel).

We predicted that when inhibition occurs 'on-time', Elbow Rotation Decline and Peak Elbow Rotation are negligible, which reflects optimal postural stabilization both before and after the unloading in a particular trial. Therefore, both measures of elbow rotation stabilization were further used to find the time optimal for Biceps brachii inhibition (see the 'Estimation of the optimal EMG inhibition' section below).

To estimate Peak Elbow Rotation and Elbow Rotation Decline in the voluntary unloading task, elbow rotation time series were first smoothed using a moving average with a window of 5 time points (8.3 ms) and a step size of 1 time point (1.7 ms) to reduce noise. The time series were then visually inspected to identify the time of maximal elbow deflection using the 'annotations' tool in MNE-Python. This step was performed manually because, in most trials, the peak elbow rotation was very small and difficult to reliably detect using automatic algorithms. The time series were then epoched into [-1.7 to 1.2] s relative to the annotated maximum elbow rotation.

Peak Elbow Rotation was calculated as the mean of baseline-corrected values within a 33 ms window surrounding the maximal elbow rotation, excluding outliers. The baseline for each trial was defined as the mean over the lowest values in a 33 ms

window (excluding outliers) in the interval [-0.35 to -0.05 s] relative to the maximum of elbow rotation

To estimate Elbow Rotation Decline, the epoched elbow rotation time series were used. Elbow Rotation Decline was defined as the difference between the mean of the lowest values in a 33 ms window (excluding outliers) from -165 ms to the start of unloading, and the mean of the highest values in a 33 ms window (excluding outliers) from -165 ms to the time points corresponding to Elbow Rotation Decline (to avoid positive elbow deflection following elbow decline). In case of negligible elbow decline, time intervals for Elbow Rotation Decline and its baseline could overlap.

Overall, Elbow Rotation Decline and Peak Elbow Rotation values were calculated individually for each trial. The resulting plots for each trial with time points used for elbow rotation peak, decline and their baselines estimation were visually inspected (see Figure 1B for example of data and baseline intervals used), and severe artifact-containing trials, preventing accurate estimation of elbow rotation measures, were detected (the number of such trials in each subject: from 0 to 5, mean=1.25, SD=1.39). These trials were excluded from all analyses using elbow rotation data.

Electromyography (EMG)

For this study, EMG recordings from the left Biceps Brachii were analyzed. Preprocessing steps followed the same protocol as in previous work by the group (Barlaam et al., 2018) and included epoching from -1 to 0.5 s relative to the unloading event, mean subtraction, and band-pass filtering in the 25-150 Hz range using a FIR filter with a Hamming window based on the group-averaged muscle Power Spectral Density. The filtered data were rectified to allow visualization of EMG inhibition as a decrease in EMG power (see Figure 2A, right panel).

The data were then log10-transformed and baseline-corrected using the -1 to -0.5 s interval. Due to the high noise level, tracking inhibition in individual trials was not feasible, but inhibition was clearly visible in the group-averaged signal (see Figure 2A, right panel). To quantify the strength of inhibition, a moving average with a 30 ms window and 33% overlap was applied to smooth the signal further.

Estimation of the EMG inhibition

Since tracking muscle inhibition in each trial was not feasible due to noise levels, we instead aimed to extract the strength of EMG inhibition during the time when its occurence was followed by optimal postural stabilization. This involved identifying the time interval at which EMG inhibition had the greatest impact on both Elbow Rotation Decline and Peak Elbow Rotation, bringing both values close to zero. The inhibition may reflect the suppression (or modulation) of the previous motor command in the elbow flexor. If so, it must occur at an optimal time - not too early, to ensure elbow

stabilization until unloading, and not too late, to prevent destabilization caused by the persistence of an old motor command. The potential timing scenarios for inhibition (early, on-time, and late) and their behavioral consequences are schematically summarized in Figure 1A below.

To investigate the mechanisms of the most efficient strategy, i.e. on-time inhibition, which is dominant in the group of adult participants (Schmitz et al., 1999), we aimed to find the time at which the occurrence of inhibition results in the lowest negative deflection (Elbow Rotation Decline) before the unloading and lowest Peak Elbow Rotation after the unloading (option 1, Figure 1A).

For this, in each subject individually we fitted a linear regression model over trials to predict EMG based on two predictors: Elbow Rotation Decline and Peak Elbow Rotation. The OLS() function from statsmodels.regression.linear_model module, statsmodels library (v. 0.14.1) was used to fit the model at each time point of the smoothed data (see above). The F-value was used as the evaluation metric for each regression model. The quality of the prediction was assessed using the coefficient of determination (R^2). The F-values were log10-transformed to normalize the distribution and baseline-corrected (-1 to -0.5 s). By this, a time point with positive F-value was considered to represent the moment where the combined influence of Elbow Rotation Decline and Elbow Rotation Peak had the strongest predictive power on Biceps Brachii EMG, associated with muscle inhibition, relative to the general baseline effect. To assess the statistical significance of the baseline-corrected F-values, we performed a permutation cluster one-sample test over subjects with time adjacency in -0.25 to 0.1 s time interval relative to the unloading.

In the imposed condition, where anticipating load release was impossible, EMG decrease occurred reflexively about 100 ms after unloading. To detect EMG decrease in each subject, the EMG signal was preprocessed similarly to the voluntary condition and baseline-corrected (-1 to -0.5 s). It was then averaged over a 30 ms window centered on the latency showing the strongest EMG decrease in the trial-averaged signal.

MRI data acquisition and preprocessing

Structural magnetic resonance imaging (MRI; voxel size 0.9 mm x 0.9 mm x 0.9 mm; TR=3500 ms, TE=2.24 ms) data were obtained from all the participants using 3T Siemens Magnetom scanner (CERMEP, France - MAGNETOM Prisma, Siemens HealthCare). The T1-weighted images were preprocessed with the ‘recon-all’ procedure from FreeSurfer software (version 6.0.0, Fischl et al., 2002), which particularly included

motion correction, intensity normalization, removal of non-brain tissue, cortical surface reconstruction, and subcortical segmentation.

The cortical surface was parcellated into 450 regions using the "HCPMMP1" atlas (Glasser et al., 2016), as implemented in MNE-Python software (v. 1.7.0, Gramfort et al., 2013). To identify brain regions involved in anticipatory motor control, contralateral to the postural left forearm, we performed a source-level MEG analysis focusing on specific regions in the right hemisphere. These regions included areas of the motor network associated with voluntary unloading in the BLLT task (Schmitz et al., 2005; Ng et al., 2010; Ng et al., 2013a; Ng et al., 2013b), see Table 1.

In addition to the cortical regions, several subcortical brain structures in the right hemisphere were included in the MEG source-level analysis. These regions were automatically parcellated using the Aseg atlas in FreeSurfer and included the cerebellar cortex and basal ganglia (caudate nucleus, putamen, and globus pallidus).

	Cortical parcellation labels from Glasser et al. (2016)
M1	R_4_ROI
SMA	R_SCEF_ROI, R_6ma_ROI, R_6mp_ROI
PM	R_55b_ROI, R_6d_ROI, R_6a_ROI
CMA	R_24dd_ROI, R_24dv_ROI
PrCu	R_PCV_ROI, R_7Am_ROI, R_7Pm_ROI
SMar	R_PF_ROI, R_Pft_ROI, R_Pfop_ROI, R_Pfm_ROI, R_PFcm_ROI
dlPFC	R_8C_ROI, R_8Av_ROI, R_i6-8_ROI, R_s6-8_ROI, R_SFL_ROI, R_8BL_ROI, R_9p_ROI, R_9a_ROI, R_8Ad_ROI, R_p9-46v_ROI, R_a9-46v_ROI, R_46_ROI, R_9-46d_ROI
IFC*	R_44_ROI, R_45_ROI, R_IFJp_ROI, R_IFJa_ROI, R_IFSp_ROI, R_IFSa_ROI, R_47l_ROI, R_p47r_ROI

Table 1. Selected regions of interest (ROIs) used for MEG cluster analysis.
Primary motor cortex, M1; supplementary motor area, SMA; premotor cortex, PM, premotor cortex; cingulate motor area, CMA; precuneus, PrCu; supramarginal gyrus, SMar; dorsolateral prefrontal cortex, dlPFC; inferior frontal cortex, IFC.
*IFC involvement was not detected in BLLT, but it was included in the directed connectivity analysis due to its well-established role in inhibitory motor control (Swann et al., 2012; Xu et al., 2016).

MEG data acquisition

Magnetoencephalography (MEG) recordings were acquired using a CTF-MEG system (CERMEP, France), equipped with 275 radial gradiometers positioned over the scalp, along with 33 reference channels for correcting ambient noise. The MEG signals were digitized at a 600 Hz sampling rate and low-pass filtered between 0 and 150 Hz. Head position was tracked continuously using three coils placed on the nasion and preauricular points before recording.

MEG sensor-level data analysis

Preprocessing steps

MEG data preprocessing and analysis were performed using MNE-python software (v. 1.7.0; Gramfort et al., 2013). Raw MEG data sessions from the voluntary unloading condition (three sessions per subject), aligned to initial head positions in each session, were concatenated. Visual inspection of head movements showed that shifts in x, y, and z coordinates did not exceed 1 cm. Detailed analysis confirmed that head position remained stable across all three coordinates during the anticipatory period (-0.5 to 0 s relative to unloading) used in the following analysis.

Independent component analysis (ICA) decomposition was performed on high-pass filtered at 1Hz data using ICA() function (number of components: 70, method: 'picard', maximum number of iterations: 1000, reference channels were included in the IC estimation). Components corresponding to biological artifacts (blinks, heart beating, muscle activity) were excluded on the basis of visual inspection of components timecourses and topographies. MEG reference channels were used to detect components contaminated by intermittent noise using find_bads_ref() function with threshold=1.5. The selected components were removed from an unfiltered copy of raw data. The average number of excluded components (mean ± SD) was as follows: EOG components: 2.06 ± 0.24; ECG components: 1.25 ± 0.56; EMG components: 1.44 ± 1.54; artificial noise components: 6.56 ± 3.46.

The raw data were then epoched in (-1.7 to 1.2 s) time window relative to the unloading. Only those trials where the moment of the start of the unloading was possible to detect and elbow rotation time series were not severely contaminated were included (number of dropped trials per subject, mean ± SD: 1.19 ± 1.18). Data of 275 axial gradiometers were selected for the analysis. Epochs were visually inspected and those contaminated by instrumental noise and myogenic artifacts were excluded (number of dropped trials per subject, mean ± SD: 2.00 ± 2.89). Several trials were additionally excluded from the analyses with elbow rotation data due to inability to

reliably estimate Peak Elbow Rotation or/and Elbow Rotation decline, see above. The final average number of trials for each subject was 86.94 ± 2.97 (mean ± SD).

For the control imposed condition, preprocessing included the same steps, with epoching performed in the time interval of -0.5 to 0.5 seconds around the load release, resulting in a total of 87.00 ± 5.55 (mean ± SD) trials per subject.

MEG source-level data analysis

Individual brain models and inverse solution

Three MRI-visible fiducial landmarks (nasion, left auricular, and right auricular) were manually positioned and used to define the head coordinate system. Individual structural MRI data were coregistered with MEG raw data using mne.gui.coregistration() tool. Single layer boundary element model (BEM) was created with 20484 vertices for the 2 hemispheres. A mixed source space was defined which combined the surface-based source space with 'ico4' spacing allowing reconstruction of 5124 cortical vertices in the two hemispheres and volume source space with 5mm spacing including cerebellum and basal ganglia structures reconstruction (see above) in the two hemispheres, comprising 1300 sources in total. Forward solution was computed for sources with minimal distance from the inner skull surface equal to 5mm.

Notch filters at 50 and 100 Hz were applied to raw data to reduce powerline noise. Data were band-pass filtered in 25-150Hz for the analysis of gamma activity and in 1-90Hz for the analysis of power in the alpha-beta range. The type of filter used in both cases was finite impulse response (FIR) filtering, with a Hamming window and zero-phase configuration. The filter length was set to 'auto' using the 'firwin' design and a padding type of 'reflect_limited'. The resulting raw data were epoched as described at the preprocessing step, and bad trials were excluded based on prior annotations.

The data rank was computed from the epoched data, with the singular values tolerance for considering non-zero values set to 1e-6, and the tolerance kind set to 'relative'. The data covariance matrix was calculated for the [-1, 0.1] time interval, an interval expected to capture the brain response associated with anticipatory motor control. It was computed using the predefined rank and the method set to 'empirical'. Since only one type of channel — gradiometers — was used and the beamformer method was applied, we avoided estimating a noise covariance matrix for source reconstruction, as its time interval would be unclear in the current setup. The unit-gain Linearly Constrained Minimum Variance (LCMV) beamformer spatial filter was

computed to optimize power orientation, with a regularization coefficient of 0.05 and the 'reduce_rank' parameter set to 'True'. The filter was then applied individually to each epoch.

Time-frequency analysis

Time-frequency analysis was performed over the full time window (-1.7,1.2 s) with symmetric padding of 0.5 s added to each side of the array. The resulting data were then cropped to the time window of interest, (-0.5,0.25 s).

For gamma power estimation, the Multitaper method was applied to the time series of individual trials and brain source data using the tfr_array_multitaper() function. The analysis was conducted in the 90-130 Hz frequency range with the 'time_bandwidth' parameter set to 4. The resulting power estimates were log10-transformed and averaged across the frequency dimension, yielding an average high-gamma power estimate for the 90-130Hz range. For periodic power estimation in the alpha-beta range, Superlets algorithm was used (https://github.com/irhum/superlets, Moca et al., 2021). For each trial and brain source, the superlets() Python function was applied to the time series within the 1-80Hz frequency range, with a base cycle set to 3. The (minimum, maximum) upper limit of orders for adaptive superlets was set to (1, 20).

The Spectparam tool (known as 'FOOOF', Donoghue et al., 2020) was then used to separate periodic activity from the total 1-80Hz power. A 2-80Hz frequency range was selected as appropriate for the Spectparam fit, based on a visual inspection of the power spectral densities of a few trial-averaged individual sources across several subjects. Periodic power for each trial and source was defined as the difference between the total power and the final aperiodic fit obtained from the Spectparam model, which was based on trial-averaged power spectra in the 2-80Hz range. For analysis, periodic power in the alpha-beta frequency range (8-30Hz) was extracted.

Correlational analyses

Previous research suggests that flexor inhibition during voluntary unloading may be linked to reduced excitability rather than increased inhibitory signaling in the brain region controlling muscle activity (Kazennikov et al., 2005; 2006). To examine whether reduced excitability in a specific brain region relates to EMG inhibition, we calculated Spearman's rank correlation coefficient between EMG inhibition (see details in Results section) and high-gamma power (averaged in the 90-130Hz range), considered a proxy for excitability. Indeed, high-gamma activity, defined as activity in a broad frequency range above 60 or 80 Hz, has been shown to correlate closely with spiking activity in both sensory (Ray et al., 2008; Ray et al., 2011; Suffczynski et al., 2014) and motor networks (Yazdan-Shahmorad et al., 2013), supporting its role as an indicator of regional excitability. The correlations were calculated for each time point (-

0.25 to 0 s) and each cortical source within the voluntary unloading right motor network (see MRI section above). To assess the statistical significance of the observed correlations, we performed a spatio-temporal one-tailed permutation cluster test. This test was used to identify positive clusters, i.e., brain regions within the motor network where a decrease in high-gamma power (indicative of reduced excitability) was associated with stronger EMG inhibition (decreased EMG power) near -0.026 s.

To estimate the possible involvement of other brain regions in the regulation of on-time inhibition via alpha- or beta-band activity, we computed a Spearman's rank correlation coefficient between periodic power and EMG inhibition in each source vertex in the right motor network, each frequency bin in the 8-30Hz range, and each time point in the (-0.25 to 0 s) time window. A spatio-temporal one-tailed permutation cluster test was again used to identify negative clusters, which would indicate higher alpha-beta range power in trials with stronger inhibition.

Additionally, to verify the involvement of subcortical regions in the regulation of inhibition, spatio-temporal one-tailed permutation cluster test was performed on the Spearman's rank correlation coefficient between the periodic power in 8-30Hz and EMG inhibition individually for the right cerebellum and basal ganglia.

Mediation analysis

To test whether gamma power (mediator, M) mediates the relationship between beta power (independent variable, X) and EMG inhibition (dependent variable, Y), a mediation analysis was conducted. The analysis focused on the peak vertex within the SMA cluster region, defined as the vertex showing the strongest correlation between gamma power and EMG inhibition within a cluster. Total (without aperiodic component subtraction) beta and gamma powers were averaged over their respective frequency bands (24-25Hz for beta and 90-130Hz for gamma) and across the time interval showing significant gamma power vs. inhibition correlation (-0.06 to -0.018 s), which also overlapped with 24-25Hz beta power vs. inhibition correlation time interval. The use of a unique time interval for both the independent variable and the mediator is justified by the fast conduction velocity of neural signals (less than 1 ms), which is below the time resolution of the current data, making it impossible to differentiate their exact timings.

The mediation analysis was performed using the mediate() function (package 'mediation', v. 4.5.0) in R, employing bootstrapping with 10,000 permutations to obtain robust estimates of the mediation effects. To account for random effects, a generalized additive model (GAM, function bam(), package 'mgcv' v. 1.9.0) with linear fixed effects (gamma power, beta power), random effects per subject (random intercepts, random beta and gamma slopes) were employed. Restricted maximum likelihood (REML) was used as the estimation method for the GAM models. The models used as inputs for the mediation analysis - models A and C' - are described in Table 2. To justify the presence

of relationships between the mediator and dependent variable, and between the independent and dependent variables, two additional models - models B and C (Table 2) - were specified.

Model	Relationship	Formula in mgcv
A	$X \rightarrow M$	Gamma ~ Beta+s(Subject,bs='re')+s(Subject,Beta,bs='re')
C'	$X + M \rightarrow Y$	Inhibition ~ Beta+Gamma+s(Subject,bs='re') +s(Subject,Beta,bs='re')+s(Subject,Gamma,bs='re')
B	$M \rightarrow Y$	Inhibition ~ Gamma+s(Subject,bs='re') +s(Subject,Gamma,bs='re')
C	$X \rightarrow Y$	Inhibition ~ Beta+s(Subject,bs='re')+s(Subject,Beta,bs='re')

Table 2. Mediation analysis models.
Inhibition: EMG inhibition; *Gamma:* gamma power averaged over 90-130Hz; *Beta:* total beta power averaged over 24-25Hz and adjusted for correlation with broad range total power (1-130Hz); *s(Subject,bs='re'):* subject-based random intercept; *s(Subject,Beta,bs='re'):* subject-specific random slope for beta power; *s(Subject,Gamma,bs='re'):* subject-specific random slope for gamma power.

Before fitting the models, beta power was adjusted by regressing out (LinearRegression() function, 'sklearn', v. 1.4.2) the total power averaged across a broad frequency range (1-130Hz) to mimic the partial correlation approach used for the Beta power vs. Gamma power correlation (see *Statistical analysis*). The resulting Beta power and Gamma power variables were further scaled between subjects to yield standardized mediation parameters. The linearity of the relationships between the dependent and independent variables was visually inspected. The Durbin-Watson d-test (dwtest() function, 'lmtest' package, v. 0.9.40) was used to test for autocorrelation in the residuals of the estimated GAM models. The test indicated the presence of significant positive autocorrelation for *model a* (DW = 1.89, p = 0.01). However, the DW value is close to 2, suggesting that the autocorrelation is mild and may not substantially affect the validity of the model. For the other models, no autocorrelation was observed (mean DW ± SD: 1.970 ± 0.002, mean p-value ± SD: 0.163 ± 0.011). To assess the presence of multicollinearity among the linear predictors in *models a and c'*, the Variance Inflation Factor (VIF) was calculated (mgcv.helper::vif.gam() function, 'mgcv.helper' package, v. 0.1.9). All VIF values were < 2, suggesting an absence of multicollinearity.

Beta bursts extraction

To extract bursts of beta activity in the vertices of interest, we used the burst detection pipeline developed by Szul et al. (2023; https://github.com/maciekszul/burst_detection). For this, time-frequency decomposition and aperiodic component separation were

performed using Superlets() and Spectrparam() as described above. One difference in the approach was a use of 0.25Hz frequency resolution in the Superlets(), to improve burst detection. Beta bursts search time and frequency range was set to -0.8 to 0.4 s and 10-33Hz, respectively. To verify that the algorithm worked correctly for bursts extraction, the resulting trial-based time-frequency plots and plots with bursts only were visually inspected and compared.

For this study, only bursts at the peak of the SMA vertex with a burst center frequency between 22-28 Hz and a burst center time within -0.077 to -0.018 seconds were considered for analysis. These bursts were individually subtracted for each trial. The time window was selected based on the beta power vs. inhibition correlation, while the frequency range (25 ± 3 Hz) was chosen to capture the strongest frequency effect observed at 25 Hz.

Beta bursts analysis

To test whether trials containing the selected bursts are associated with stronger EMG inhibition, we averaged baseline-corrected and 30-ms smoothed EMG power timecourses (see section *Estimation of the optimal EMG inhibition* above) across these trials. A one-tailed permutation cluster test with time adjacency was then performed across subjects in the -0.25 to 0.05 s window relative to unloading, to determine if there was a significant decrease in EMG power, i.e. stronger inhibition, relative to 0.

For further analyses, trials containing bursts were aligned to the times of their burst centers. For the baseline, an equal number of trials with the lowest beta power within the same time and frequency range used for burst selection were also aligned to the burst center times.

To identify brain regions associated with inhibitory bursts in the SMA, we calculated the directed connectivity measure, Phase Slope Index (PSI), using the phase_slope_index() function from the MNE-Python. PSI was computed between the peak SMA vertex and vertices in the right motor network. The spectrum for PSI estimation was calculated using Morlet wavelets with 4 cycles. PSI was computed in the 22–28 Hz frequency range separately for trials with bursts and baseline trials.

A spatio-temporal one-tailed permutation cluster test was conducted to contrast PSI-based connectivity in burst trials vs. baseline trials, aiming to identify brain regions targeting the SMA specifically during bursts. Separate cluster tests evaluated connectivity from the cerebellum and basal ganglia to SMA. To assess the involvement of additional regions identified in the literature, PSI connectivity was also tested from the left M1 to the peak of the right M1 cluster region, and from the right cerebellum and right basal ganglia to the peak of the right M1 cluster region. All analyses were performed within the -0.05 to 0 s time window relative to SMA burst centers.

In the identified cluster regions, beta burst probability was calculated for burst trials and baseline trials. It was computed at each time and frequency point in each vertex as the ratio of trials with bursts to the total number of trials. To improve estimate stability, this ratio was averaged across vertices within each cluster. To test whether beta burst probability increased in trials with SMA bursts in the regions defined from PSI connectivity analysis, we conducted a one-tailed permutation cluster test. The test examined if the beta burst probability averaged over the 22-28Hz frequency range increases in burst trials compared to baseline trials within the -0.05 to 0.05 s time window relative to SMA burst centers.

Statistical analysis

To check the assumptions of linear regression models, several diagnostic tests were performed. The Shapiro-Wilk test (shapiro() function, scipy.stats, v. 1.7.3) was used to assess the normality of the residuals. The Durbin-Watson test (durbin_watson() function, statsmodels.stats.stattools, v. 0.13.5) was employed to check for autocorrelation in the residuals. Homoscedasticity was tested with Breusch-Pagan Lagrange Multiplier test (het_breuschpagan() function, statsmodels.stats.api, v. 0.13.5). Multicollinearity was tested using the Variance Inflation Factor (VIF) (variance_inflation_factor() function, from statsmodels.stats.outliers_influence, v. 0.13.5).

To assess the relationship between neural activity and behavioural parameters at individual time, frequency, and spatial points, we calculated Spearman's rank correlation coefficient (spearmanr() function, scipy.stats, v. 1.7.3). Spearman's correlation was chosen due to the potential presence of non-linear relationships between the pairs of variables studied.

To estimate the relationship between alpha-beta band (8-30Hz) and high gamma activity (90-130Hz) with adjusting for the total power in the broad frequency range (see Supplementary methods, Spaak et al., 2012), we calculated partial Spearman's correlation coefficient (partial_corr() function, from pingouin, v. 0.5.3) with total power averaged in the broad frequency range (1-130Hz) taken as a covariate. This approach, while having its limitations, allowed us to treat average power variability between trials as a common factor between two frequency ranges. This variability is primarily driven by the aperiodic component, which is correlated between the two frequency bands.

To perform cluster analysis, group-level statistics, or select a common set of vertices across all subjects (e.g., SMA cluster region or right motor network), the timecourses or correlation coefficients calculated for individual brain models were morphed to the template brain, 'fsaverage', using the compute_source_morph()

function in MNE-Python. For 'fsaverage', BEM and source spaces were created with the same parameters as those used for the sample data.

A non-parametric permutation cluster one-sample t-test (using permutation_cluster_1samp_test() for data with time dimension only and spatio_temporal_cluster_1samp_test() for the rest cases implemented in MNE-Python) was used for cluster analyses. A total of 1024 permutations were performed to generate a null distribution for cluster-level inference. Clusters were formed based on spatio-temporal, spatio-time-frequency, time-frequency, or time-only adjacency. One- or two-tailed tests were used depending on the hypothesis being tested (see the corresponding Methods section for details of each individual test). We applied Threshold-Free Cluster Enhancement (TFCE) for cluster-level statistics on two-dimensional time-frequency data (starting value: 0, step size: 0.2). To reduce computational costs, for data with spatial adjacency we used a strict cluster-forming threshold based on the t-distribution with a p-value of 0.001. To validate this approach, we performed a permutation cluster test for the correlation between gamma power and EMG inhibition using both the TFCE-based threshold and the cluster-based threshold of p=0.001. Both analyses revealed a significant cluster with overlapping spatial distributions, confirming the validity of the chosen statistical thresholds.The 'hat' variance regularization implemented in MNE-Python was applied to estimate the t-test statistics, compensating for implausibly small variances.

Results

Behavioural data

Group average of standardized elbow rotation and EMG modulation over time with between-subject variability is shown at Figure 2A. The distributions of Peak Elbow Rotation and Elbow Rotation Decline in each subject over trials were significantly different from normal (Shapiro-Wilk test, $p < 0.05$ in all subjects), while their median and SD were overall low in all the participants, as compared to their reflex-like median peak elbow rotation in the control imposed condition (voluntary/imposed *100%; Peak Elbow Rotation, median ± SD: 5.46 ± 7.44%; Elbow Rotation Decline, median ± SD: -0.43 ± 2.04%; see Figure 2B for individual variability). The observed 5% for the average ratio between maximal elbow deflections in the voluntary vs. imposed condition is consistent with the previously reported 8% in adults (Barlaam et al., 2012). Such a pattern is expected for the voluntary unloading in adult participants, who exhibit mature anticipatory postural control keeping elbow deflection low.

To determine the optimal timing of EMG inhibition in the Biceps brachii, we aimed to identify when inhibition occurred 'on-time,' leading to better elbow

stabilization, as indicated by smaller deviations from zero in both Peak Elbow Rotation and Elbow Rotation Decline (Figure 1A; see Methods for details). While Peak Elbow Rotation reflects the magnitude of elbow deflection following load-lifting, Elbow Rotation Decline might be associated with too early anticipatory inhibition: stronger Elbow Rotation Decline correlated to stronger EMG inhibition around -0.06 s and -0.08 s (One-sample t-test for Spearman R's: $t=7.5$, $p<0.001$ and $t=5.2$, $p<0.001$, respectively). In addition, no Elbow Rotation Decline was observed in the imposed condition, where anticipation is not possible.

To identify inhibition time associated with best elbow stabilization, we used F-values derived from linear regression models that predicted EMG inhibition based on the two elbow parameters at individual time points (see Methods). A permutation cluster test revealed a significant difference in baseline-corrected F-values, most pronounced at three time points (-0.086, -0.066, and -0.026 s relative to unloading), indicating moments when EMG activity is strongly related to elbow rotation variables (Figure 2C, left panel). The R^2 values for the linear regression models at each time point are presented in Figure 2C, left panel. Inspection of the correlation coefficients of the two variables (Figure 2C, right panel) revealed that the effect around -0.086 s and -0.066 s was mainly driven by a positive correlation between Elbow Rotation Decline and EMG, suggesting that earlier inhibition, i.e. more negative EMG, was associated with elbow rotation destabilization before the unloading. In contrast, R^2 around -0.026 s was explained by a negative correlation between EMG and Elbow Rotation Decline and a positive correlation between EMG and Peak Elbow Rotation, suggesting that stronger (more negative) inhibition was related to lower Peak Elbow Rotation and less Elbow Rotation Decline, thus overall better postural stabilization both before and after the unloading.

The time interval around -0.026 s in the Biceps brachii EMG was thus identified as the optimal window for inhibition during the voluntary unloading task, as it was associated with the best postural stabilization. Notably, this interval aligns well with previous studies on BLLT, which indicate that efficient anticipatory postural control is linked to inhibition occurring within the 50 ms interval preceding the onset of unloading (Viallet et al., 1987). The "on-time" inhibition measure, referred to as "EMG inhibition" below, was therefore estimated as the average of preprocessed and baseline-corrected (-1 to -0.5 s) Biceps brachii EMG power within a 30 ms window centered around -0.026 s. Stronger EMG inhibition, indicated by a more negative EMG value, suggests that in that trial inhibition occurred at the optimal moment for anticipatory postural control. Conversely, weaker inhibition, indicated by a more positive EMG value, would reflect that inhibition in that trial was either early (likely occurring around -0.066 or -0.086 s) or late. In contrast to elbow deflection parameters, Biceps Brachii Inhibition values were generally normally distributed (Shapiro-Wilk test,

p>0.05 in 14 of 16 subjects) and showed greater variability across trials within participants (mean ± SD: -0.018 ± 0.034; see Figure 1C).

To validate the use of linear regression in this analysis, we tested if the key assumptions were met for the subject-based models at -0.026 s time point. The linearity of the relationship between independent and dependent variables was confirmed through visual inspection of scatterplots. In all the subject-based models, the residuals were normally distributed (Shapiro-Wilk tests, p > 0.05 in all participants), did not show positive or negative autocorrelation supporting their independence (Durbin-Watson test, group-averaged statistics: 1.96 ± 0.19 (SD), min: 1.68, max: 2.36), and did not show the presence heteroscedasticity (Breusch-Pagan test, p > 0.05 for all participants). To ensure that there was no multicollinearity, the Variance Inflation Factor (VIF) was calculated. Both independent variables had acceptable VIF values below 5, indicating that the predictors were not highly correlated (group-averaged VIF: 1.05 ± 0.05 (SD), min: 1.00, max: 1.19).

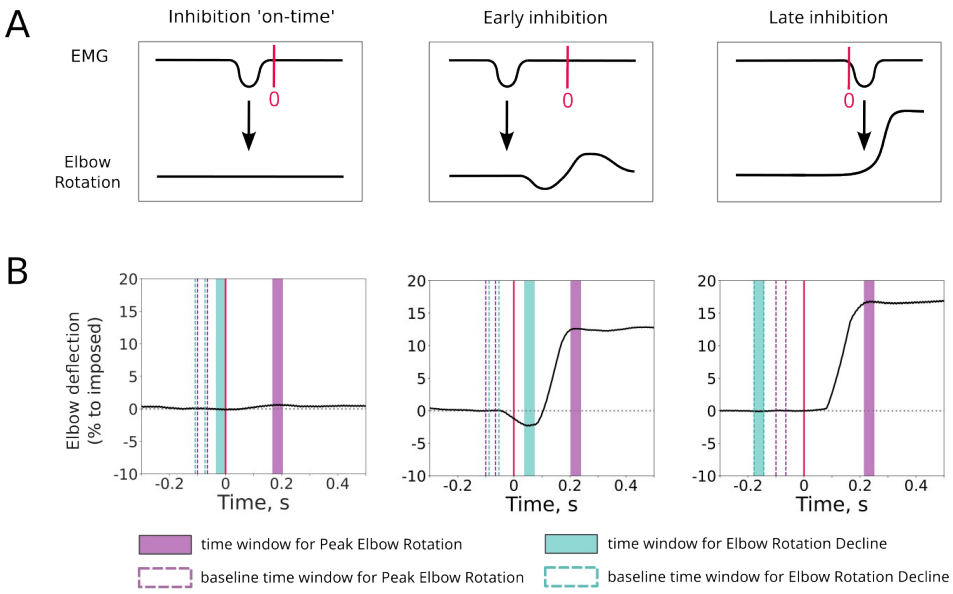

Figure 1. Detection of elbow deflection and its hypothetical relationship to the timing of Biceps brachii inhibition. **A:** Schematic representation of three core possible situations for Biceps Brachii inhibition timing and its consequences on elbow rotation. See detailed explanation in Methods (section *Estimation of the optimal EMG inhibition*). **B:** Examples of single trials illustrating the time intervals used for estimating Peak Elbow Rotation and Elbow Rotation Decline.

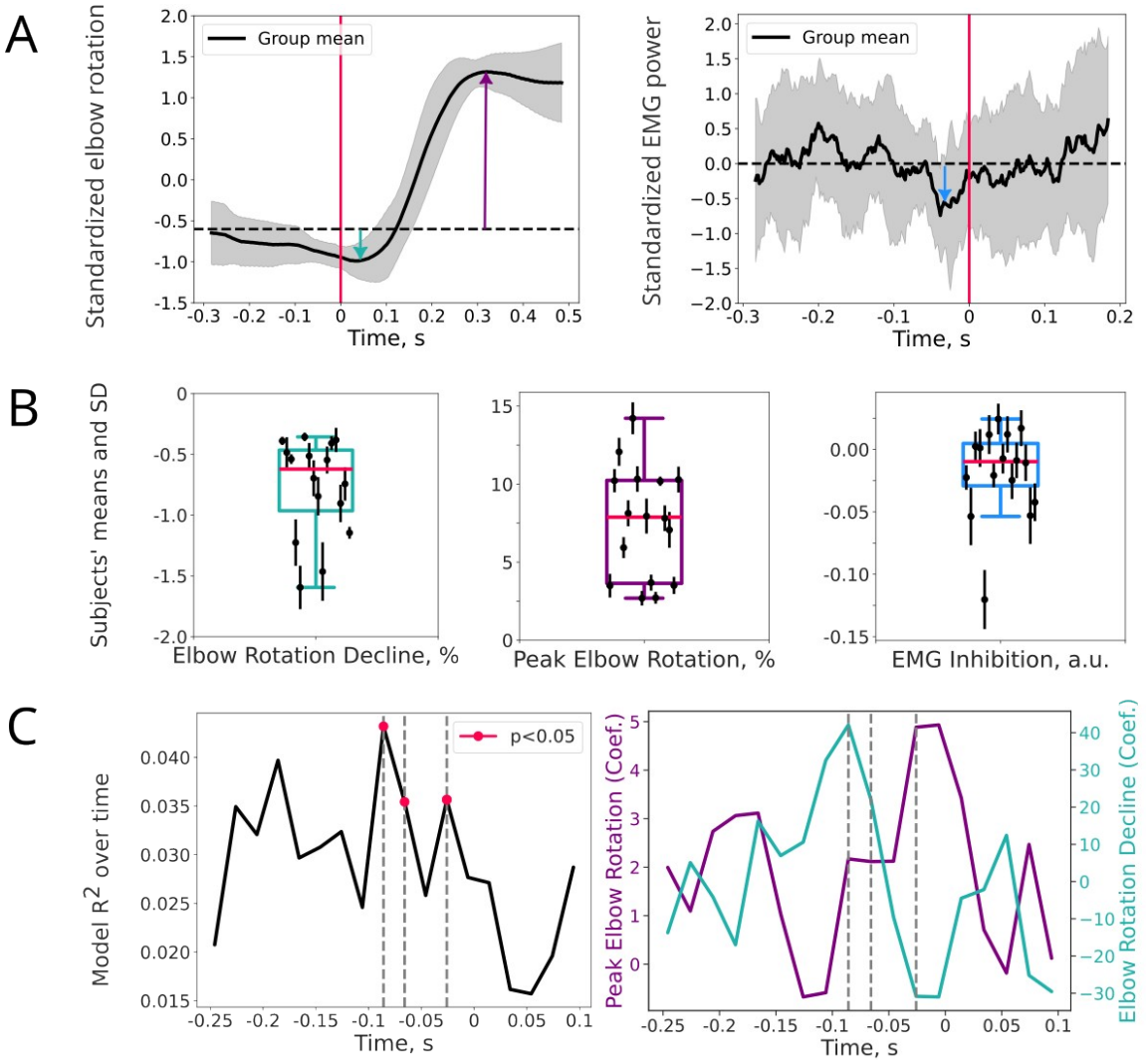

Figure 2. Behavioural data-based hypotheses and analysis. **A:** Standardized (subtracted mean, divided by standard deviation (SD)) Biceps Brachii EMG and elbow rotation modulation over time, relative to the start of voluntary unloading (vertical red line): trial- and group-average (black thick line) and SD (filled gray area). Colored arrows schematically demonstrate magnitudes of three estimated behavioural measures: left panel – the Elbow Rotation Decline (green) and Peak Elbow Rotation (purple); right panel – the EMG inhibition (blue). **B:** Mean (black dots) and SD (black whiskers) of the three behavioral measures for each subject. The boxplots are representing the between-subjects variability: red horizontal line is median; edges of the box are first and third quartiles (Q1 and Q3), whiskers are 1.5 times the interquartile range. **C:** Averaged over subjects outputs of the linear regression models, calculated at each time point individually (dependent variable: EMG power, independent variables: Peak Elbow Rotation, Elbow Rotation Decline). Left panel: R^2 values; right panel: linear regression coefficients for Peak Elbow Rotation (purple) and Elbow Rotation Decline (green) from the models. Red markers and grey dashed lines indicate time points where the F-value corresponded to $p<0.05$.

MEG data

Correlation with EMG inhibition in contralateral motor network

To determine whether reduced excitability in a specific brain region is associated with an EMG decrease, we performed a permutation cluster test on correlations between high gamma power (90-130Hz), indicative of greater neural excitability (Murthy & Fetz, 1996; Ray et al., 2008; Lundqvist et al., 2016; Riehle et al., 2018; Brazhnik et al., 2021), and EMG inhibition across vertices of the right anticipatory motor network (see Table 1). The test revealed a significant effect (cluster time window: -0.25 to 0 s), with a pronounced positive effect in the medial frontal cortex,, corresponding to the medial SMA (Figure 2A). This suggests that stronger EMG inhibition around -0.026 s is linked to decreased high gamma power in the preceding time window (-0.06 to -0.018 s), roughly consistent with the latency of nerve conduction (Spiecer et al., 2013; Entakli et al., 2014).

Estimating high-gamma activity in motor tasks using non-invasive methods may raise concerns about muscle activity contamination. We however argue that this is unlikely in our setup. First, MEG studies (e.g., Muthukumaraswamy et al., 2010) have shown detectable gamma oscillations (60-100 Hz) in motor areas like M1. Second, the anticipatory period lacked visible movement, which only became apparent after unloading began. Additionally, as described in Methods, participants exhibited minimal head motion (<1 cm), indicating limited phasic effects. While tonic muscle activity could still contribute, the use of a beamformer for source localization reduces broadband gamma artifacts (Manyukhina et al., 2021). Combined with the use of correlation as a relative measure and a spatially precise effect in the SMA, located on the medial surface where tonic muscle contamination is not expected to be strong, we claim that the observed EMG inhibition-high-gamma power correlation reflects a genuine neural process.

In contrast to the anticipatory cortical network, the permutation cluster test did not reveal a significant correlation between EMG inhibition and high-gamma power in the right basal ganglia or cerebellum.

Similarly, under the imposed unloading condition, no significant positive correlation was detected between high-gamma power and the reflex-like EMG decrease, unlike in the voluntary unloading condition.

Cluster region-based analysis in SMA

The analysis described above allowed us to identify a cluster region where stronger EMG inhibition was associated with reduced high-gamma power. We then investigated whether increased alpha and/or beta activity in this region was also linked to the observed effects - stronger EMG inhibition and reduced gamma power. Such a relationship would suggest that alpha-beta power might regulate the level of

excitability in this region, thereby influencing the activity of the muscles it controls.

In the medial SMA cluster identified from the previous analysis, a permutation cluster test revealed a significant negative correlation between periodic power and EMG inhibition, pronounced across a broad high beta frequency range (18-25Hz) and an extended time window (-0.228 to -0.018 s), as shown in Figure 3B. Notably, within this range, the time interval used for EMG inhibition calculation overlapped with the 24-25Hz power correlation (red dashed line, Figure 3B). This correlation indicates that higher beta power occurs during trials with stronger 'on-time' inhibition. Given the short latency between SMA stimulation and muscle response (mean MEP latency: 15.7ms in Spiecer et al., 2013; 22.6ms in Entakli et al., 2014), this late high-beta effect likely reflects a direct inhibitory influence rather than an earlier lower-frequency correlation component, which may be linked to preparatory beta-band synchronization facilitating efficient inhibitory communication. However, investigation of this effect is beyond the scope of the present study.

To examine the relationship between late high-beta activity and gamma power within the 10 vertices of the SMA cluster region, we computed a partial Spearman's correlation coefficient between 24-25Hz and 90-130Hz power, averaged across frequency and over the gamma correlation cluster time interval (-0.06 to -0.018 s), while controlling for total 1-130Hz-averaged power to account for shared variance, as previously applied in Spaak et al., 2012. Notably, to estimate this correlation, we used a common LCMV spatial filter applied to data filtered between 1-150Hz, which ensured comparable capture of both low- and high-frequency activity. Individual subjects' correlation coefficients were significantly negative (one-sample t-test: $t = -7.16$, $p < 0.001$), indicating that stronger high beta power is associated with a greater reduction in high gamma power. A significant negative correlation was also observed when periodic beta power (obtained by subtracting the aperiodic component) was directly correlated with high-gamma power using Spearman's correlation. However, the effect size for this correlation and the t-test comparing the correlation to 0 were smaller (one-sample t-test: $t = -2.17$, $p = 0.046$).

Since the effect was observed in the SMA, but not in M1 where the correlation with EMG inhibition was initially expected, we additionally tested whether a significant correlation existed between EMG inhibition and high gamma power decrease and 8-30Hz power increase in the M1 elbow region, based on literature-defined coordinates. Talairach coordinates for the left elbow area (Biceps & Triceps brachii) from Lotze et al. (2000) and Plow et al. (2010) ([-28, -24, 64] and [-29, -25, 63], respectively) were averaged and converted to MNI305 space, yielding [32, -20, 66] in the right hemisphere. The M1 elbow region was defined as the peak vertex and its five adjacent vertices, forming a six-vertex label (see Figure 3A, lower panel). In this region, the permutation cluster test did not reveal a significant correlation between EMG inhibition and either high-gamma power or 8-30Hz power.

We further investigated whether other regions might exhibit alpha or beta power related to inhibition. To test this, we performed another permutation cluster test on the correlation between 8-30Hz power and EMG inhibition across the right motor network. No significant effect was observed for this correlation, either in the right motor network, basal ganglia, or cerebellum.

Mediation analysis

A mediation analysis was conducted to examine whether the effect of high beta power on inhibition is mediated through high gamma power. In the defined model, beta power was the independent variable (X), EMG inhibition was the dependent variable (Y), and gamma power served as the mediator (M). The GAM models, referred to as models A, B, C, and C' (see Methods, Mediation analysis section), included both linear fixed effects and random effects. The following significant relationships were found: beta power predicted gamma power (*model A*: estimate (β) = -0.138, standard error (SE) = 0.027, 95% confidence interval (CI) = [-0.190,-0.085], t = -5.18, p < 0.001), gamma power significantly predicted EMG inhibition (*model B*: β = 0.106, SE = 0.035, 95% CI = [0.037,0.175], t = 3.061, p = 0.002), beta power significantly predicted EMG inhibition (*model C*: β = -0.069, SE = 0.025, 95% CI = [-0.120,-0.019], t = -2.725, p = 0.007), and beta power and gamma power together predicted EMG inhibition (*model C'*: beta power: β = -0.056, SE = 0.025, 95% CI = [-0.108,-0.005], t = -2.188, p = 0.029; gamma power: β = 0.092, SE = 0.035, 95% CI = [0.022,0.162], t = 2.609, p = 0.009).

The results of the mediation analysis are presented in Table 3, see also Figure 3C. The analysis revealed a statistically significant mediation effect (Average Causal Mediation Effect, ACME) of gamma power on the relationship between beta power and EMG inhibition, as well as a significant total effect. However, the direct effect (Average Direct Effect, ADE) of beta power on EMG inhibition, after accounting for the mediator, was also significant. The proportion of the total effect of beta power on EMG inhibition that was explained by the mediator accounted for 22%, suggesting a partial mediation.

	Estimate (β)	95% CI	p-value
ACME	-0.013	[-0.02, 0.00]	0.006 **
ADE	-0.057	[-0.11, -0.01]	0.027 *
Total effect	-0.069	[-0.12, -0.02]	0.007 **
Proportion mediated	0.183	[0.04, 0.67]	0.013 **

Table 3. Mediation analysis results
*<0.05, **<0.01

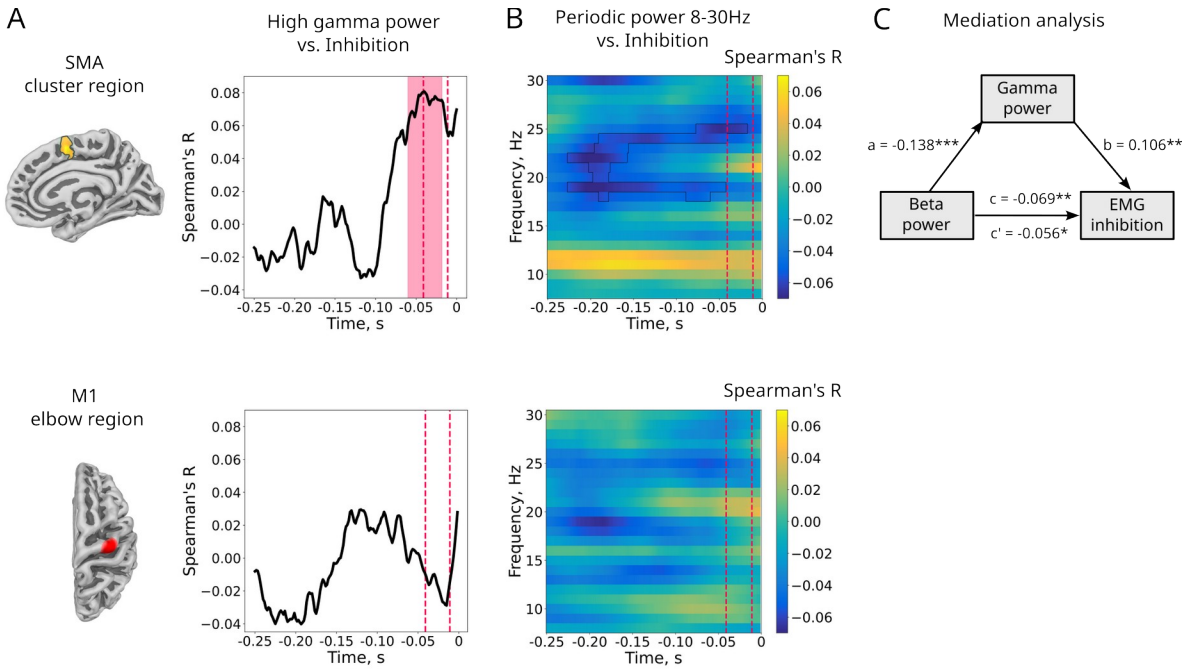

Figure 3. A: Upper panel: a significant cluster showing the correlation between high gamma power (averaged in the 90-130 Hz range) and EMG inhibition (estimated within a 30 ms window around -0.026 s, marked by red dashed lines), localized in the medial SMA (MNI305 peak: [8, 3, 52]). The thick black line represents the time course of the correlation within the cluster. The red transparent area highlights the (-0.06 to -0.018 s) time window corresponding to the significant cluster. Lower panel: the right M1 elbow region (MNI305 peak: [32, -20, 66]), defined using coordinates from the literature (see the text above), and its timecourse for the correlation between high gamma power and inhibition (not significant). **B:** Results of the permutation cluster test, limited to the SMA cluster region (upper panel) or M1 elbow region (lower panel) and showing the Spearman's correlation coefficient (R) between periodic power in the 8-30Hz range and EMG inhibition (estimated in 30ms around -0.026 s, red dashed lines). Thin black lines highlight significant clusters. **C:** Mediation analysis results, demonstrating the relationships between Beta power (independent variable), Gamma power (mediator), and EMG inhibition (dependent variable). The linear regression coefficients for each path in the model, along with their statistical significance, are presented. *p<0.05; **p<0.01; ***p<0.001

Beta bursts analysis

Brain beta activity is often represented in the form of bursts in humans (Little et al., 2019; Lundqvist et al., 2024), which complicates the estimation of connectivity measures (Lundqvist et al., 2024). To identify brain regions involved in sending

inhibition signal to the medial SMA, we first applied a burst detection algorithm to the SMA peak timecourse (see Methods). Beta bursts were selected if their centers fell within the interval from (-0.077 to -0.018 s), corresponding to the period when beta power correlated to EMG inhibition close to inhibition time estimation. As the strongest frequency effect during this interval occurred at 25 Hz, we focused on bursts within the 22-28Hz range. The percentage of trials containing bursts was low, with a mean ± SD of 11.6 ± 1.9%. The absolute number of trials with bursts was similarly low (mean ± SD: 10.1 ± 1.78). Notably, the number of trials with bursts remained consistent when the time-frequency signal was extracted from the 10 vertices of the medial SMA cluster region and averaged for burst detection.

Beta bursts and EMG inhibition

To test whether trials with detected beta bursts also exhibit stronger EMG decreases at the time of inhibition, we performed a one-sample permutation cluster test on the EMG power averaged over these trials. The test revealed a significant EMG decrease at -0.026 s ($p = 0.008$; Figure 4A), corresponding to the previously defined time of inhibition. However, when the same number of trials was selected based on the strongest beta power averaged in the same time and frequency window, no significant EMG decrease was observed ($p > 0.18$). This suggests that beta bursts better explain the data than beta power alone.

Connectivity analysis

To identify brain regions sending inhibitory signals to the medial SMA, we performed directed connectivity analysis using the PSI within the selected burst frequency range. PSI was calculated between the right motor network and the peak SMA vertex over the trials containing bursts (centered around burst centers) and contrasted with PSI computed over the same number of baseline trials that did not contain bursts.

The PSI contrast revealed two significant clusters through a permutation cluster test: one near the elbow representation in M1 ($p = 0.043$) and another in the middle PFC ($p = 0.004$) (Figure 4B). The direction of the PSI contrast indicated connectivity from the M1 and PFC clusters to the medial SMA. The M1 cluster spanned from -0.043 to -0.020 s, and the PFC cluster from -0.040 to -0.010 s, relative to the SMA burst center (Figure 4C, upper panel). No significant clusters were found in the right basal ganglia or cerebellum.

To investigate the relationship between the observed PFC and M1 clusters during the time when they both drive the SMA, we estimated the PSI contrast between

these clusters across vertices and time. When averaged over the vertices and the time interval of their overlapping effect on the SMA, PSI contrasts were compared to zero across subjects. This revealed significant connectivity from the PFC to the M1 cluster region (Figure C, lower panel; one-sample t-test, T = 2.33, p = 0.034).

If connectivity from the PFC to SMA and from the M1 to SMA exists, an increase in beta burst probability in the PFC and M1 cluster regions, temporally aligned with bursts in the SMA, would also be expected. Indeed, a permutation cluster test revealed an increase in beta burst probability in both the M1 and PFC cluster regions close in time to the SMA burst centers in trials containing bursts compared to no burst trials (M1: -0.012 to 0.050 s; PFC: -0.021 to -0.005 s relative to the SMA burst center) (Figure 4D).

Bimanual coordination suggests a potential link between the M1 regions in the right and left hemispheres. To test for connectivity from the left M1 to the identified right M1 cluster, we computed the PSI between all vertices in the left M1 (as defined by the anatomical atlas; Glasser et al., 2016) and the peak vertex of the right M1 cluster. A permutation cluster test contrasting PSI scores in the 22-28Hz range between trials with bursts and trials without bursts did not reveal a significant effect.

Given that the connection between M1 regions is hypothesized to involve subcortical pathways (Viallet et al., 1992), we also tested directed connectivity using PSI contrasts from the right basal ganglia and cerebellum to the right M1 cluster. While no significant clusters were observed for basal ganglia to M1 connectivity, there was a tendency for a cluster of cerebellum-to-M1 connectivity when estimated in the -0.05 to 0 s range relative to burst center (T=3.74, p=0.138; one voxel at -0.028 s, MNI coordinates: [20, -90, -35]).

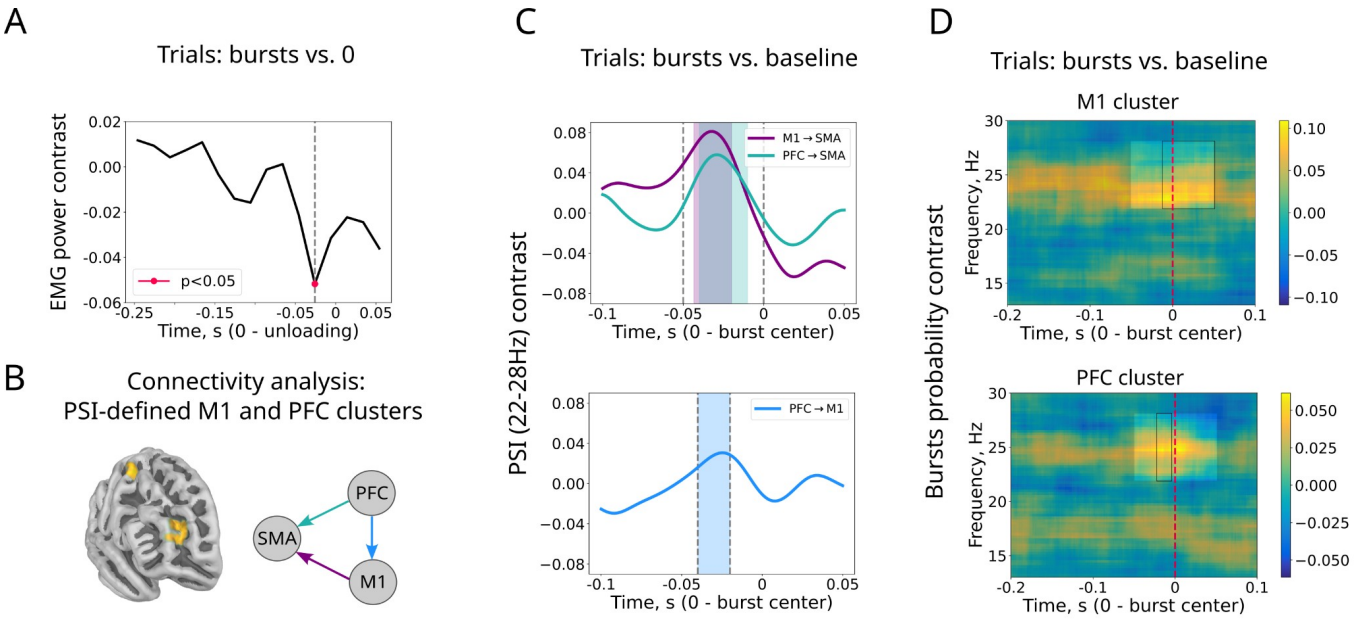

Figure 4. Results of beta bursts analysis. **A:** Results of the permutation cluster test showing a decrease in EMG power at the time corresponding to the inhibition time

interval in trials with beta bursts. **B:** Localization of significant clusters (M1: 3 vertices, MNI305 peak: [38,-8,56]; PFC: 10 vertices, MNI305 peak: [31,47,11]) identified based on the PSI contrast between trials with SMA bursts and no burst trials. The schematic representation highlights connectivity directions between the SMA, M1, and PFC cluster regions. **C:** PSI contrast timecourses for M1-to-SMA, PFC-to-SMA, and PFC-to-M1 connectivity. The upper panel shows significant time intervals (shaded areas) within the cluster analysis window (dashed lines), while the lower panel highlights the time-averaging window where the contrast was significantly different from zero (shaded areas, dashed lines). **D:** Time-frequency representation of beta burst probability dynamics in the M1 and PFC cluster regions, relative to SMA burst centers. Bright squares indicate the interval of interest (-0.05 to 0.05 s and 22-28Hz) used for cluster analysis over time (averaged in 22-28Hz), with thin black lines marking significant time clusters.

Discussion

In this study, we investigated the neural mechanisms of anticipatory muscle inhibition preventing forearm destabilization following voluntary load-lifting. We found that stronger EMG inhibition at the optimal time correlated with reduced high-gamma power reflecting decreased excitability in the SMA. Stronger inhibition also correlated with increased high-beta power in the SMA, with the relationship partially mediated by the decrease in high-gamma power. Directed connectivity analysis on SMA high-beta bursts indicated that M1 and the middle PFC transmit high-beta signals to the SMA. These findings suggest that timely anticipatory inhibition in the BLLT is driven by high-beta bursts, which inhibit the SMA and release its control over the elbow flexors.

In voluntary unloading, lifting a load alters applied forces, while timely anticipatory inhibition aims to counteract the disturbance of equilibrium. In adults, inhibition in the elbow flexor is time-locked to the activity of the same muscle in the load-lifting arm, suggesting a central timing command that coordinates both arms (Paulignan et al., 1989; Massion, 1992). However, studies in children show that such timed coordination is established through prolonged maturation (Schmitz et al., 2002; Barlaam et al., 2012). Furthermore, Bolzoni et al. (2015) demonstrated that APA can be modulated without affecting voluntary movement, suggesting a separation of the two commands at the SMA level. These data indicate that APA is generated by a separate

command that accounts for the upcoming movement and forearm disturbance and timely adjusts muscle tone accordingly.

Though APA in adults is time-locked to motor arm activity, there is variability left in the latency of anticipatory inhibition (Barlaam et al., 2012). We found that optimal forearm stabilization occurs when Biceps brachii inhibition happens 26±15 ms before unloading, closely matching the average anticipatory inhibition latencies reported in adults (25 ms, Dufossé et al., 1985; 32 ms, Barlaam et al., 2012).

The relationship between anticipatory motor network excitability and elbow flexor inhibition in the BLLT was explored by Kazennikov et al. (2005; 2006). Using transcranial magnetic stimulation (TMS) they showed reduced M1 excitability, measured by Motor Evoked Potentials (MEPs), during anticipatory inhibition. However, the same link between MEPs and EMG decrease was also present in control conditions, suggesting that the observed effect was not APA-specific.

To assess neural excitability with MEG, we measured high-gamma (90-130Hz) power, which closely correlates with neural spiking (Murthy & Fetz, 1996; Ray et al., 2008; Lundqvist et al., 2016; Riehle et al., 2018; Brazhnik et al., 2021). Surprisingly, we found no link between stronger EMG inhibition and reduced excitability in M1, likely due to EMG baseline normalization ensuring the inhibition reflected time-specific effect. However, stronger EMG inhibition correlated with reduced medial SMA excitability, which was characteristic of the voluntary condition as was not observed in the control condition. This relationship suggests that the SMA contributes to muscle tone control during load holding, while this control is reduced in anticipation of force changes.

The role of SMA in BLLT has been consistently demonstrated in MEG and fMRI studies (Schmitz et al., 2005; Ng et al., 2011; 2013). APA impairments were linked to contralateral SMA lesions, which allowed authors to suggest that SMA contributes to gating posture stabilization circuits (Viallet et al., 1992), consistent with the current findings.

Previous studies have also questioned the extent of M1 involvement in APA during voluntary unloading (Kazennikov et al., 2005). Ng et al. (2013) suggested that SMA may mediate APA via direct corticospinal projections. Indeed, SMA has precise and reliable somatotopic maps (He et al., 1995; Strother et al., 2012), while its corticospinal projections are half as extensive as M1's (Dum & Stick, 1991). In humans, TMS stimulation of SMA induced MEPs in arm muscles during motor tasks, with latencies and amplitudes comparable to those of M1 (Spieser et al., 2013; Entakli et al., 2013). These findings suggest that SMA can directly contribute to precise forearm muscle control. SMA-to-muscle communication in the beta-band has been proposed to support precise force control when the forthcoming force production is anticipated (Chen et al. 2013; Entakli et al., 2013; Spieser et al., 2013). It was speculated that the

apparently superior corticospinal projections from the SMA in humans compared to non-human primates (Maier et al., 2002) may have evolved to enable advanced anticipatory corrections for coordinating complex movements (Chen et al., 2013). During load-holding in anticipation of forearm destabilization, the SMA may play a role in taking partial selective control over elbow flexors, as reflected in the early correlation effect shown in Figure 4B. The release of this control during SMA inhibition, seemingly corresponding to a higher-frequency effect peaking at 25 Hz, facilitates a smooth transition to a new postural state.

We demonstrated that anticipatory elbow flexor inhibition was mediated by stronger high-beta, but not alpha activity, in the SMA. To our knowledge, this is the first direct evidence of the inhibitory effect of beta activity on muscle function. The high-beta effect latency (~20 ms) closely matched SMA stimulation MEP latency (15.7 ms, Spiecer et al., 2013; 22.6 ms, Entakli et al., 2014). Reduced high-gamma power partially mediated this relationship, suggesting that high-beta activity contributes to EMG inhibition by decreasing SMA excitability. While not always consistent (Confais et al., 2020), this aligns with studies showing an inverse relationship between high-gamma/spiking and beta activity in sensorimotor areas (Ray et al., 2008; Lundqvist et al., 2016; Riehle et al., 2018), and supports the contrasting roles of beta in inhibition and high-gamma in excitation (Ray & Maunsell, 2011; Lundqvist et al., 2024).

If anticipatory inhibition during voluntary unloading results from suppressed SMA activity, one question remains: which brain region/network is transmitting the inhibitory signal. To address bursty beta signal connectivity (Lundqvist et al., 2024), data were centered on high-beta bursts near inhibition. Directed connectivity revealed that the M1 elbow area and middle PFC (Brodmann area 46, BA46) transmit a high-beta signal to the SMA, with burst probability increasing in these areas. While either region could potentially inhibit SMA activity, this seems unlikely, as neither is part of the network underlying action cancellation (Borgomaneri et al., 2020). Additionally, the burst frequency of M1 (~22.5Hz) does not match that of the SMA effect (~25Hz, see Figures 2B, 3D). M1 likely serves as a source of proprioceptive signals transmitted to the SMA (Nasrallah et al., 2019). Alternatively, since lesions of M1 output abolish APA (Viallet et al., 1992), M1 may relay motor command from the left hemisphere to adjust postural control accordingly. While no link was found between left and right M1, communication likely occurs at a subcortical level (Viallet et al., 1992) in a different bursting regime, complicating estimation. BA46's burst frequency (~25Hz) matches SMA activity in our study, while some studies relate its activity to action inhibition processes (Cieslik et al., 2012). However, rather than exerting a direct inhibitory function, this area appears to facilitate the integrity and maintain the tone of the inhibitory network in a task- and muscle-specific manner (Buschman, et al., 2012; Hasan et al., 2013; Khan et al., 2024).

If not M1 or middle PFC, which region could transmit the inhibitory signal for anticipatory postural control? While our results do not provide a direct answer, we speculate that the SMA subarea can be involved. The classical “SMA” is divided into two areas with distinct connectivity and functions: SMA-proper and pre-SMA (Tanji, 1994). SMA-proper is somatotopically organized, projects to the spinal cord, and connects with M1 (Coull et al., 2016), consistent with the muscle control discussed above.

SMA-proper, however, lacks direct connections with prefrontal regions, which the pre-SMA is rich in, particularly BA46, while pre-SMA has no direct connections with M1 (Luppino et al., 1993). Along with IFC, pre-SMA contributes to the inhibitory network for action stopping, driven by beta-band synchronization (Coull et al., 2016; Swann et al., 2012; Leunissen et al., 2022) and selectively inhibits motor activation patterns based on task instructions (Burle et al., 2004; Carbonnell et al., 2013). Since both SMA subareas contribute to motor command timing (Hoffstaedter et al., 2012; Coull et al., 2016), it can be assumed that the pre-SMA transmits a timely inhibitory signal to SMA-proper, either directly via adjacent arm fields (Luppino et al., 1993) or indirectly through the basal ganglia (Wadsey et al., 2022).

One limitation of this study is the small sample size, which prevents conclusions about the involvement of subcortical areas, such as the basal ganglia and cerebellum, in anticipatory inhibition due to the lower signal-to-noise ratio for MEG deep sources (Attal & Schwartz, 2013). Additionally, while burst-centering partially addressed connectivity issues, the high variability of bursts and potential non-linear effects highlight the need for new connectivity approaches (Lundquist et al., 2024).

In conclusion, this study enhances the understanding of APA mechanisms in bimanual load-lifting.We found that anticipatory inhibition is linked to high-beta bursts in the SMA, likely through SMA suppression, emphasizing the SMA's role in forearm postural correction. Alongside, M1 and middle PFC transmit high-beta signals that support SMA-to-muscle communication. Although pre-SMA may be responsible for the signal suppression, further studies are needed to identify its exact source. Future studies should use connectivity-based methods (Kim et al., 2010) to differentiate SMA subareas and explore their roles, along with M1, in APA, particularly under greater behavioral variability, such as in children.

Acknowledgments

We would like to thank Maciej Szul, James Bonaiuto, Jérôme Prado, Franck Lamberton, and Sarah Le Diagon for their invaluable contributions to this study.